WATER RESOURCES RESEARCH, VOL. 37, NO. 5, PAGES 1143–1154, MAY 2001

Tracer tests in a fractured dolomite 3. Double-porosity, multiple-rate mass transfer processes in convergent flow tracer tests

Sean A. McKenna and Lucy C. Meigs
Geohydrology Department, Sandia National Laboratories, Albuquerque, New Mexico

Roy Haggerty
Department of Geosciences, Oregon State University, Corvallis, Oregon

Abstract. Convergent flow tracer tests conducted in the Culebra dolomite (Rustler Formation, New Mexico) are analyzed with both single- and multiple-rate, double-porosity models. Parameter estimation is used to determine the mean and standard deviation of a lognormal distribution of diffusion rate coefficients as well as the advective porosity and longitudinal dispersivity. At two different test sites both multirate and single-rate models are capable of accurately modeling the observed data. The single-well injection-withdrawal test provides more precise estimates of the mass transfer parameters than the convergent flow tracer tests. Estimation of the multirate distribution parameters is consistent across locations for the two types of tests. Limits of resolution are calculated for the multirate distribution, and these limits explain the precision with which the standard deviation of the multirate distribution can be estimated. These limits also explain the necessary increase in the advective porosity for the single-rate model at one location and not the other. Implications of the multirate mass transfer model at time and length scales greater than those of the tracer tests include the instantaneous equilibrium of a significant fraction of the matrix and the possibility of a fraction of the diffusive porosity not reaching an equilibrium solute concentration at long times.

1. Introduction

A number of single-well injection-withdrawal (SWIW) and convergent flow tracer tests (CFTT) have been conducted in the Culebra dolomite member of the Rustler Formation in the vicinity of the Waste Isolation Pilot Plant (WIPP) in southeastern New Mexico [*Meigs and Beauheim*, this issue]. These tracer tests were conducted with the goal of better characterizing the physical transport parameters of the Culebra dolomite. Modeling of the SWIW test results indicates that matrix diffusion is an important transport process within the Culebra [*Altman et al.*, 2000]. The conceptual model of matrix diffusion within the Culebra was extended from the conventional double-porosity single-rate model to a continuous lognormal distribution of diffusion rate coefficients [*Haggerty et al.*, this issue]. The multirate diffusion model was shown to provide superior model fits to the observed SWIW test data relative to the conventional single-rate model [*Haggerty et al.*, this issue].

The signature of multirate diffusion processes in a CFTT is more difficult to discern than in a SWIW test because of added complexity in the physics governing the flow system. Specifically, this added complexity may be due to (1) tailing caused by flow field heterogeneity, a process the SWIW test is designed to mitigate, and (2) the sensitivity of the tracer transport results to advective porosity. In this paper we examine the applicability of the multirate diffusion model to a subset of the multiwell CFTTs.

Paper number 2000WR900333.
0043-1397/01/2000WR900333$09.00

At the H-19 and H-11 hydropads, multiple injection wells were centered around the central pumping well (multiwell testing). In this paper we examine a single pathway (i.e., one injection well to the pumping well) at each hydropad. As used in this paper, a CFTT is defined as a test with a single injection well and a single withdrawal well. Prior to tracer injection, the pumping rate has been maintained in the withdrawal well for sufficient time to allow velocities to be considered steady state within the domain of the tracer test. A slug of tracer is injected into this steady state convergent flow system from a second well located a distance R away from the pumping well. Immediately following the injection of the tracer, a chaser of Culebra brine (containing no tracer) is injected to flush the injection well of any remaining tracer. At the end of the chaser injection the injection rate is reduced to zero for the remainder of the tracer test. The discharge at the pumping well remains constant throughout the tracer and chaser injections and throughout the collection of tracer data (up to 50 days).

Tracer tests with two or more wells have been used by a number of researchers to estimate groundwater flow and transport parameters over a volume of aquifer between the injection and recovery wells. As pointed out by *Moench* [1989], a strength of these multiple-well tests is that 100% recovery of the injected tracer is theoretically possible thus providing confidence in the conceptual model used to analyze and model the tracer recovery. Numerous tracer tests have been conducted with the goal of determining dispersivity [e.g., *Novakowski et al.*, 1985; *Moench*, 1989; *Welty and Gelhar*, 1994]. Other researchers have used multiwell tracer tests to determine the effective porosity and anisotropy of the flow system [e.g.,

Sánchez-Vila and Carrera, 1997]. Multiwell tracer tests can also provide information on sorption and diffusion processes in fractured rock [*Maloszewski and Zuber*, 1993; *Moench*, 1995; *Haderman and Heer*, 1996; *D'Alessandro et al.*, 1997; *Garcià Gutiérrez et al.*, 1997].

Tracer breakthrough curves (BTCs) in multiwell tests can generally be described as exhibiting a relatively rapid rise to a peak concentration and then a decline in concentration after the peak. The latter portion, or tail, of the BTC may be of the same timescale as the rise in concentration or considerably longer. The length of the tail is controlled by flow field heterogeneity (typically modeled with a dispersivity value) and factors that would retard the transport of solute relative to pure advective flow, such as diffusion from a fracture to the matrix or sorption. While the concept of several discrete rates of diffusion has been proposed for modeling transport in fractured systems [*Neretnieks and Rasmuson*, 1984; *Moench*, 1995; *Haggerty et al.*, this issue, and references therein], construction of a continuous multirate mass transfer model from CFTT data has not previously been reported.

The goal of this paper is to elucidate the processes responsible for mass transfer in the Culebra dolomite. Toward this goal, we are interested in developing a model of mass transfer between fracture and matrix porosity or, more generally, between porosity that can be accessed by advection (advective porosity) and porosity that can only be accessed by diffusion (diffusive porosity) and then testing that model on data acquired in a number of CFTTs. In this paper we will (1) extend the methodology of estimating distributions of multirate mass transfer rates from the SWIW to the CFTT, (2) model the observed CFTT breakthrough curves with a multirate diffusion model, (3) examine the uniqueness of the estimated model and compare the results to those obtained with conventional single-rate models, and (4) discuss the extension, or scaleup, of the multirate model to scales larger than that of the tracer test (i.e., the scale of repository performance assessment).

2. Multirate Transport Modeling in Two Well Systems

The multirate diffusion transport model described by *Haggerty et al.* [this issue] is extended here to work with CFTTs. The multirate model [*Haggerty and Gorelick*, 1995] enables mass transfer to be modeled with a continuous distribution of diffusion rate coefficients. A distribution of diffusion rate coefficients may arise from variability in matrix block sizes and cross-sectional area of the pore space normal to the direction of diffusion and tortuosity. The multirate mass transfer model presented here is similar to that described by *Cunningham et al.* [1997] and *Haggerty and Gorelick* [1998]. Diffusion is assumed to occur along one-dimensional pathways within the matrix blocks, and it is assumed that mass transfer properties are homogeneous along each pathway and that each pathway is independent of all other pathways. The pathways and matrix blocks can be any shape as long as the diffusion rate coefficients form a continuous distribution. In this work we employ a lognormal distribution of diffusion rate coefficients for reasons discussed by *Haggerty and Gorelick* [1998] and for direct comparison to SWIW tracer test results [*Haggerty et al.*, this issue].

In the CFTTs considered here, a steady state convergent-flow field is obtained by pumping from an extraction well. Tracer injection occurs as a pulse/slug into the convergent flow field at an injection well located at some radial distance away from the pumping well. A chaser of clean (no tracer) fluid is injected immediately following the tracer injection to ensure that no tracer is left in the injection borehole. The aquifer is assumed to be fully confined with constant thickness in all directions and to have spatially isotropic and homogeneous flow and transport properties. These assumptions define a radially symmetric flow field around the injection and pumping wells. Mechanical mixing due to small-scale variations in the flow field is approximated with a longitudinal dispersivity term. Because of the convergent flow field, transverse dispersion is negligible. Given the high gradients imposed by the pumping well (0.3–3.0 m/m [see *Meigs and Beauheim*, this issue]), the regional gradient (0.01–0.001 m/m) plays no role. Under these conditions the process of solute transport in a radial flow system is described by

$$\frac{\partial c_a}{\partial t} + \int_0^\infty b(\alpha_d) \frac{\partial \hat{c}_d(\alpha_d)}{\partial t} d\alpha_d = \frac{1}{r}\frac{\partial}{\partial r}\left(\frac{r\alpha_L|v|}{R_a}\frac{\partial c_a}{\partial r}\right) - \frac{v}{R_a}\frac{\partial c_a}{\partial r}, \tag{1}$$

where the distribution of diffusion rates is represented as a probability density function of diffusion rate coefficients $b(\alpha_d)$, defined by a lognormal distribution [see *Haggerty and Gorelick*, 1998; *Hollenbeck et al.*, 1999]:

$$b(\alpha_d) = \frac{\beta_{\text{tot}}}{\sqrt{2\pi}\sigma_d\alpha_d} \exp\left\{\frac{[\ln(\alpha_d) - \mu_d]^2}{2\sigma_d^2}\right\}, \tag{2a}$$

where

$$\alpha_d = D_a/l^2, \tag{2b}$$

$$\beta_{\text{tot}} = \frac{\phi_d R_d}{\phi_a R_a}. \tag{2c}$$

The terms in (1) through (2c) are defined in the notation list. Note that (1) and (2) are those used in the analysis of the SWIW tests [*Haggerty et al.*, this issue]

A distribution of mass transfer rates arising from variation in block sizes is geologically more plausible than the single matrix block size ("sugar cube") conceptualization employed in standard double-porosity models. Equation (2) not only defines this distribution of diffusion rate coefficients, lognormal in this work, but also provides the critical link between the diffusion rate coefficients and the solute storage capacity of the diffusive porosity associated with each rate coefficient. Equation (2) ties each diffusion rate coefficient α_d to a specific volume of storage. This volume is specified as a fraction of the total storage capacity of the medium β_{tot} and is expressed as a function of the diffusion rate coefficient $b(\alpha_d)$. For nonsorbing tracers, $\beta_{\text{tot}} \equiv \phi_d/\phi_a$. Also, variability in α_d is due to variability in both l, which controls the volume to surface area ratio of the diffusive porosity, and the tortuosity of the pore space.

The pore water velocity in (1) during the pumping period is given by

$$v = -\frac{Q_{\text{out}}}{2\pi r \phi_a b}. \tag{3}$$

Q_{out} and b are defined in the notation section list. We also assume that the velocity in (3) is constant. The boundary conditions for use with (1) for conditions of radially convergent flow (pumping) are

$$\frac{\partial c_a}{\partial r} = 0, \qquad r = r_w, \tag{4a}$$

$$c_a = 0, \qquad r \to \infty. \tag{4b}$$

Initial conditions for radially convergent flow are that concentrations (both advective and diffusive) at every point are initially identical to those at the end of the injection period. Note that (4a) is a necessary boundary condition for outflow.

The time derivative of the spatially averaged solute concentration in the matrix is given by

$$\frac{\partial \hat{c}_d(\alpha_d)}{\partial t} = \frac{1}{l}\int_0^l \frac{\partial c_d(\alpha_d)}{\partial t}\,\partial z, \qquad 0 < \alpha_d < \infty. \tag{5a}$$

The concentration at a point within the diffusive porosity is given by a solution of the diffusion equation:

$$\frac{\partial c_d(\alpha_d)}{\partial t} = D_a \frac{\partial^2 c_d(\alpha_d)}{\partial z^2}, \qquad 0 < \alpha_d < \infty. \tag{5b}$$

The boundary conditions for diffusive mass transfer are that the concentration at the edge of the diffusive porosity is equal to the concentration in the advective porosity and that the concentration gradient in the center of the diffusive porosity or the internal end of the pore is zero:

$$c_d(\alpha_d, z = l) = c_a, \qquad 0 < \alpha_d < \infty, \tag{5c}$$

$$c_d \frac{\partial c_d}{\partial z}(\alpha_d, z = 0) = 0, \qquad 0 < \alpha_d < \infty. \tag{5d}$$

To solve these equations, we use the approach developed by *Haggerty and Gorelick* [1995, 1998] where a series of first-order equations are used in place of (5a) and (5b) [see *Haggerty*, 2000]. These equations are solved in the Laplace domain and then numerically inverted back to the time domain. The resulting solution for c_d from the first-order equations is mathematically identical to that which would be obtained if solving the above equations directly.

Boundary conditions and fluid fluxes must also be specified at the injection well. Pore water velocity during the injection of the tracer and chaser fluid at a radius r away from the injection well is given by

$$v = \frac{Q_{\text{inj}}}{2\pi r \phi_a b}. \tag{6}$$

The boundary conditions for use with (1) under radially divergent flow are

$$c_a - \alpha_L \frac{\partial c_a}{\partial r} = c_{\text{inj}}, \qquad r = R_{\text{iw}}, \tag{7a}$$

$$\frac{\partial c_a}{\partial r} = 0, \qquad r \to \infty. \tag{7b}$$

The combined shape of the injected tracer and chaser within the aquifer is assumed to be unaffected by the convergent flow field during the time of injection. In general, this assumption remains valid if (1) the ratio of the volume of fluid injected to the volume of fluid contained within a single pore volume within the area defined by the two wells is small and (2) the ratio of fluid velocity caused by injection to fluid velocity due to pumping is large at the location of the injection well. These two constraints can be expressed as [after *Guvanasen and Guvanasen*, 1987]:

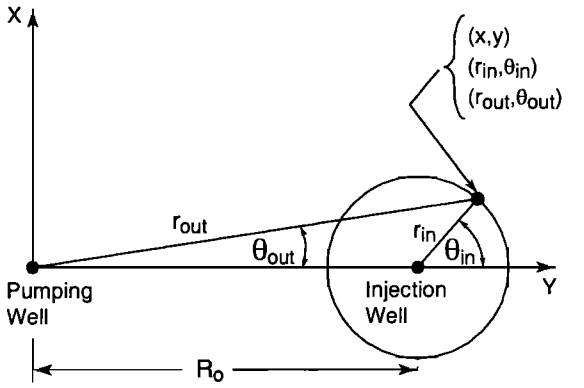

Figure 1. Schematic diagram of polar coordinate transformation from coordinates with respect to the injection well to coordinates with respect to the pumping well.

$$\frac{Q_{\text{inj1}}T_{\text{inj1}} + Q_{\text{inj2}}T_{\text{inj2}}}{b\phi_a \pi R_0^2} \ll 1, \tag{8a}$$

$$\frac{Q_{\text{inj}}R_0}{Q_{\text{out}}R_{\text{iw}}} \gg 1, \tag{8b}$$

respectively, where Q_{inj1} and Q_{inj2} refer to the injection rates of the tracer and chaser, respectively, T_{inj1} and T_{inj2} refer to the elapsed time of injection for the tracer and chaser respectively, and R_0 and R_{iw} are the distance between the injection and pumping well and the radius of the injection well, respectively. The injection rate denoted as Q_{inj} in (8b) is taken as the larger of the two injection rates (tracer or chaser), and Q_{out} refers to the discharge rate of the pumping well.

We will use the equations described above to test the conceptual model of multirate diffusion against observed tracer test data, but first it is necessary to devise a means of modeling the movement of tracer along the transport pathway from the injection well to the pumping well.

A three-step process is used to determine the breakthrough curve at the pumping well after the initial injection of tracer and chaser. The first step is to transform the postinjection concentration distribution from polar coordinates centered on the injection well (r_{in}, θ_{in}) to polar coordinates centered on the pumping well (r_{out}, θ_{out}). The second step is to reduce the dimensionality of the problem through azimuthal averaging. The final step in simulating the breakthrough curve is to model the transport through the aquifer to the pumping well under a radially convergent-flow field with the multirate diffusion model described in (1) through (5). Completion of these three steps provides a semianalytical solution for the BTC at the pumping well.

Step one involves transformation of the polar coordinates from the injection well to the pumping well. Figure 1 shows the relationship between the polar coordinate system with respect to the two wells along with an intermediate Cartesian coordinate system. The transformations from the injection well coordinate system to the pumping well coordinate system are

$$r_{\text{out}} = \sqrt{R_0^2 + 2R_0 r_{\text{in}} \cos\theta_{\text{in}} + r_{\text{in}}^2}, \tag{9a}$$

Table 1. Fixed Parameters for Convergent Flow Tracer Tests

Parameter	H-11[a]		H-19[b]	
	Low Pumping Rate	High Pumping Rate	High Pumping Rate	Low Pumping Rate
Number of data	107	75	77	67
Pumping rate, m^3/s	2.23×10^{-4}	3.76×10^{-4}	2.74×10^{-4}	1.57×10^{-4}
Tracer injection time, s	1974	1998	960	1698
Tracer injection rate, m^3/s	9.57×10^{-5}	9.5×10^{-5}	2.06×10^{-4}	1.17×10^{-4}
Chaser injection time, s	3810	3840	780	1410
Chaser injection rate, m^3/s	9.76×10^{-5}	9.71×10^{-5}	2.16×10^{-4}	1.19×10^{-4}
Diffusive porosity	0.16	0.16	0.147	0.147
Tortuosity	0.11	0.11	0.09	0.09
Aquifer thickness, m	4.4	4.4	4.4	4.4
Aqueous diffusion coefficient, m^2/s	7.9×10^{-10}	8.2×10^{-10}	8.2×10^{-10}	8.0×10^{-10}
Distance between wells, m	20.9	20.9	12.2	12.2

[a]H-11 data are for the H-11b3 to H-11b1 pathway. The low and high pumping rate data are from the round 1 and round 2 injections, respectively. See *Meigs and Beauheim* [this issue] for additional details.
[b]The H-19 data are for the H-19b7 to H-19b0 pathway. The high and low pumping rate data are from the round 1 and round 3 injections, respectively. See *Meigs and Beauheim* [this issue] for additional details.

$$\theta_{out} = \tan^{-1}\left(\frac{r_{in}\sin\theta_{in}}{R_0 + r_{in}\cos\theta_{in}}\right). \quad (9b)$$

Second, we reduce the dimensionality from two to one. Solute transport toward the pumping well as shown in Figure 1 would require solution of a system of integrodifferential equations in r_{out}, θ_{out}, and t. Azimuthal averaging can eliminate θ_{out} from this transport problem [*Zlotnik and Logan*, 1996]. Azimuthal averaging takes all concentrations at a distance r from the pumping well and averages them. In a formation with uniform thickness, advective porosity, and hydraulic conductivity all mass at a given radial distance from the pumping well will experience the same velocity and similar dispersion as it moves toward the well. Therefore all concentrations at a distance r from the pumping well can be averaged, and transport can be simulated in one dimension rather than two. The azimuthally averaged concentration at the end of the injection period, time = t_0 (beginning of convergent flow only period), is given by [*Zlotnik and Logan*, 1996]:

$$C(r_{out}, t_0) = \frac{1}{2\pi}\int_{-\pi}^{\pi} c_a(r_{out}, \theta_{out}, t_0)\, d\theta_{out}, \quad (10)$$

where r_{out} [L] is the distance from the pumping well and θ_{out} is the angle between the mass at r_{out} and the axis intersecting the pumping and injection wells. It is not necessary to integrate (10) over the entire interval $[-\pi, +\pi]$ but only over the interval where there is nonzero concentration. Azimuthally averaged concentrations are also obtained for the diffusive porosity. After the azimuthal averaging of concentrations, transport to the pumping well is modeled using (1) through (5).

3. Convergent Flow Tracer Test Simulations

Two pumping-injection well pairs are analyzed, and each well pair is analyzed at two different pumping rates. The H-11 and H-19 pathways (H-11 (H-11b3 to H-11b1) and H-19 (H-11b7 to H-11b0)) were selected because high-quality data were available for both the high and low pumping rates [see *Meigs and Beauheim*, this issue, see Table 1, Figures 3 and 4]. Each pair of injection-withdrawal wells provides a full set of benzoic acid tracer data for each of two different pumping rates. Additionally, these pathways are the longest duration data sets and thus provide the best defined breakthrough curve tails. The different benzoic acid tracer tests will be referred to by the hydropad name and the relative pumping rate for the remainder of this paper (e.g., H-19 high). The parameters that are set as fixed values in the models are given in Table 1. All fluid and tracer injections and withdrawals were done across the full aquifer thickness; however, hydraulic and tracer testing has shown that flow within the upper portion of the Culebra is insignificant [*Meigs and Beauheim*, this issue]. Therefore all flow and transport is modeled as occurring in the lower 4.4 m of the Culebra. The tracer injection is not considered to be an instantaneous injection but is defined as a square wave over the time of injection. Further details regarding the physical setup and data collection of the tracer tests are given by *Meigs and Beauheim* [this issue].

3.1. Experimental Data

The H-11 low pumping rate test (H-11 low) was run at a constant pumping rate for approximately 25 days after injection of the tracer. During this time period, 107 samples were collected and analyzed for concentration. For the higher pumping rate test (H-11 high) a total of 75 samples were collected over 14 days to define the breakthrough curve. These samples and the upper and lower limits of the 95% confidence interval based on analytical error are shown in Figure 2. All BTC concentration data shown in this paper are normalized by the injection concentration (C/C_0). The cumulative mass recovered for both of these tests is greater than 55% [*Meigs and Beauheim*, this issue, Table 3].

For the H-19 low tracer test, 67 samples collected over 47 days were used in the parameter estimation. For the H-19 high test, approximately 29 days of observed data were used in the modeling results presented here (total of 77 data points). The H-19 BTCs and the 95% confidence interval based on analytical error are shown in Figure 3. The cumulative mass recovery values for these tests are greater than 90% [*Meigs and Beauheim*, this issue, Table 3].

3.2. Parameter Estimation

Parameter estimation applied to the multirate diffusion model discussed in section 2 is used to provide an optimal fit of

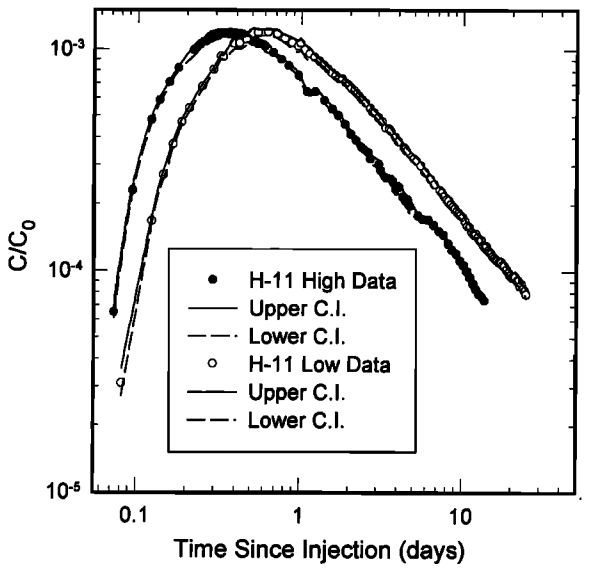

Figure 2. Observed breakthrough curve data and the limits of the 95% confidence intervals (CI) for the two H-11b3 to H-11b1 tracer tests.

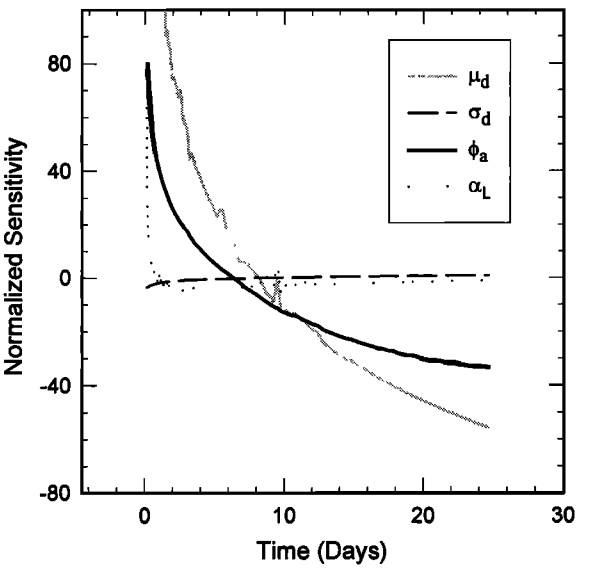

Figure 4. Normalized sensitivities of the breakthrough curve model to each of the four estimated parameters. Sensitivities from the H-11 low test are shown as an example.

the model to the observed data. The parameter estimation minimizes the root mean square error (RMSE) between the log of the observed data and the log of the predicted concentration. Errors are calculated on the logs of the concentrations in order to apply more weight to the late time, low-concentration data where the effects of mass transfer are most significant. Four parameters are estimated: the mean ln diffusion rate coefficient μ_d, the standard deviation of the ln diffusion rate coefficient distribution σ_d, the advective porosity ϕ_a, and the longitudinal dispersivity α_L. The parametric expression of diffusion rate coefficients used here is a lognormal distribution fully characterized by the mean and standard deviation. In addition to the four parameters, normalized sensitivity of the results to each estimated parameter is calculated.

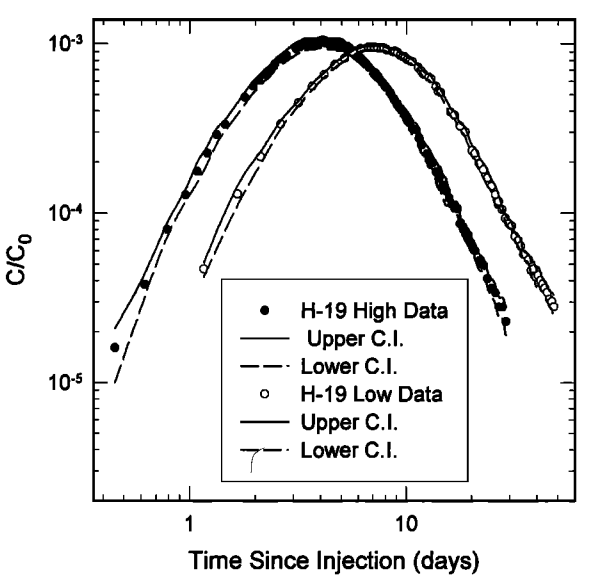

Figure 3. Observed breakthrough curve data and the limits of the 95% confidence intervals for the two H-19b7 to H-19b0 tracer tests.

The inverse parameter estimation model creates a matrix containing the sensitivity of concentration change with respect to each parameter for each observation time. The entries of this Jacobian may be normalized to allow comparison of parameter sensitivities through time and between different parameters [*Harvey et al.*, 1996]:

$$J_{ij} = \frac{p_j}{\sigma}\frac{\partial C_i}{\partial p_j}, \tag{11}$$

where J_{ij} is the normalized sensitivity of the modeled concentration at the ith time to the jth parameter, C_i is the ith component of the vector of normalized concentrations through time, p_j is jth component of the vector of estimated parameters, and σ is the estimated standard deviation for the concentration observations. Here we assume that errors are uncorrelated and due to measurement error rather than model error, and thus we use RMSE in (11) as a measure of σ. The Jacobian is a useful instrument for investigating the sensitivity through time of the model to the estimated parameters [e.g., *Wagner and Harvey*, 1997] and provides insight into the correlation between estimated parameters.

The normalized sensitivities of the H-11 low test are shown as an example of normalized sensitivities in the CFTTs (Figure 4). Examination of the normalized sensitivities (Figure 4) shows that the model of the CFTT is relatively insensitive to the values of σ_d and α_L after the time of peak concentration (approximately 0.6 days for the H-11 low test). Beyond this time the model is only sensitive to μ_d and ϕ_a, which appear to show positive correlation (Figure 4).

The estimated parameter values and the RMSE statistic obtained with the multirate model are given for the H-11 and H-19 tests in Table 2. The 95% confidence intervals in Table 2 are approximated as +/−2 standard deviations about the estimated value. For σ_d, ϕ_a, and α_L the confidence interval is taken about the natural log of the estimated value as these three parameters are estimated in natural log space within the parameter estimation algorithm. Examination of Table 2 shows that the RMSE values are all relatively small, indicating that

Table 2. Multirate Parameter Estimation Results for Convergent Flow Tracer Tests[a]

Test	n	μ_d $\pm 2\sigma$ Range	σ_d $\ln(\sigma_d \pm 2\sigma)$ Range	ϕ_a $\ln(\phi_a \pm 2\sigma)$ Range	α_L $\ln(\alpha_L \pm 2\sigma)$ Range	RMSE
H-11 low	107	−17.7	1.3	1.3×10^{-3}	3.4	0.09
		±0.9	0.3 ± 0.7	−6.6 ± 0.8	1.2 ± 0.3	
		−18.6, −16.8	0.7, 2.6	6.1×10^{-4}, 2.8×10^{-3}	2.5, 4.5	
H-11 high	75	−17.2	1.1	6.2×10^{-4}	3.0	0.12
		±1.3	0.1 ± 0.2	−7.4 ± 0.6	1.1 ± 2.6	
		−18.5, −15.9	0.9, 1.4	3.4 ± 10^{-4}, 1.0×10^{-3}	0.2, 39.3	
H-19 low	67	−16.2	5.5	3.7×10^{-3}	1.0	0.12
		±0.6	1.7 ± 3.5	−5.6 ± 0.2	0.0 ± 0.9	
		−16.8, −15.6	0.2, 180.2	2.6×10^{-3}, 5.7×10^{-3}	0.4, 2.4	
H-19 high	77	−15.2	5.5	8.5×10^{-4}	1.1	0.13
		±0.9	1.7 ± 2.5	−7.1 ± 0.02	9.5×10^{-2} ± 0.7	
		−16.1, −14.2	0.4, 68.9	8.3×10^{-4}, 8.6×10^{-4}	0.5, 2.2	

[a] For columns 3–6, read heads and entries from top to bottom, respectively.

the models provide a good fit to the observed data. Figures 5 and 6 compare the model results to the observed data for the H-11 and H-19 CFTTs, respectively. From Figures 5 and 6 it can be seen that because of fitting the log of the concentrations, the models approximate the data best at times after the peak concentration when diffusion of solute back out of the diffusive porosity into the advective porosity is the dominant mass transfer process.

3.3. Discussion of Results

Results shown in Figures 5 and 6 are based on estimated lognormal distributions of diffusion coefficients. At both hydropads the tracer test conducted at the lower pumping rate produces a lower estimate of the mean diffusion rate (μ_d). This result demonstrates that longer tests are able to observe slower diffusion rates. The cumulative diffusive porosity volume as a function of diffusion rate coefficient as determined from the inverse parameter estimation using the multirate model is shown in Figure 7 for both rounds of tests at both hydropads. Examination of Figure 7 shows that for the two hydropads the estimated distribution of diffusion rate coefficients is similar from one pumping rate to the other. However, the estimated distributions for the H-11 and H-19 hydropads differ significantly. Similar results were observed in the evaluation of the SWIW tests [*Haggerty et al.*, this issue].

All of the CFTT models estimate μ_d and ϕ_a with relatively high precision (tight confidence intervals). The precision of the σ_d estimates is much higher for the H-11 tests than for the H-19 tests. This difference is examined below in terms of the portions of the multirate distribution that can be resolved during the tests. Relatively larger confidence intervals are estimated for α_L in the H-11 high test. This imprecise estimate is caused by the rapid transport of the tracer to the pumping well (peak concentration is achieved in less than 9 hours after injection) and the insensitivity of the models to α_L beyond the time of peak concentration. Longer times to peak concentration in the H-11 low and H-19 tests allow for more precise determination of α_L.

We place limits on the range of diffusion rate coefficients that can be observed in the CFTT by using the inverse of the diffusion rate coefficient as a characteristic time for diffusion. We make the conservative assumption that a 2-order-of-

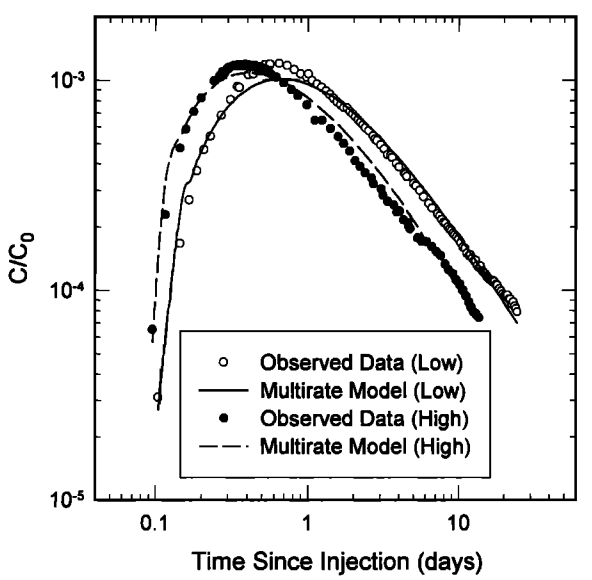

Figure 5. Multirate diffusion transport model fits to the H-11 data for both pumping rates.

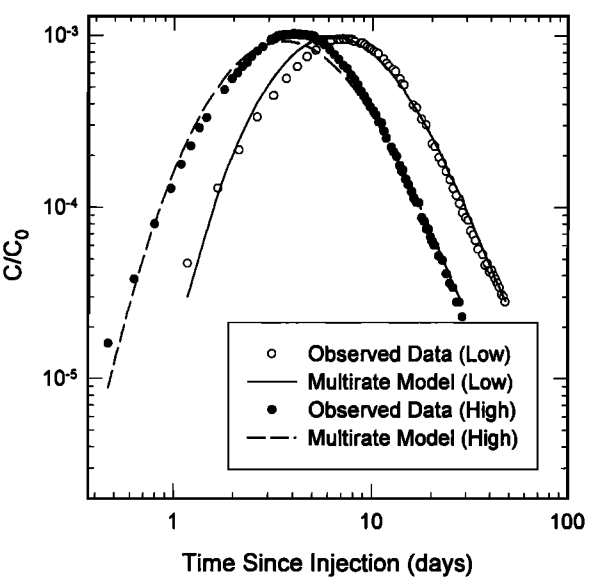

Figure 6. Multirate diffusion transport model fits to the H-19 data for both pumping rates.

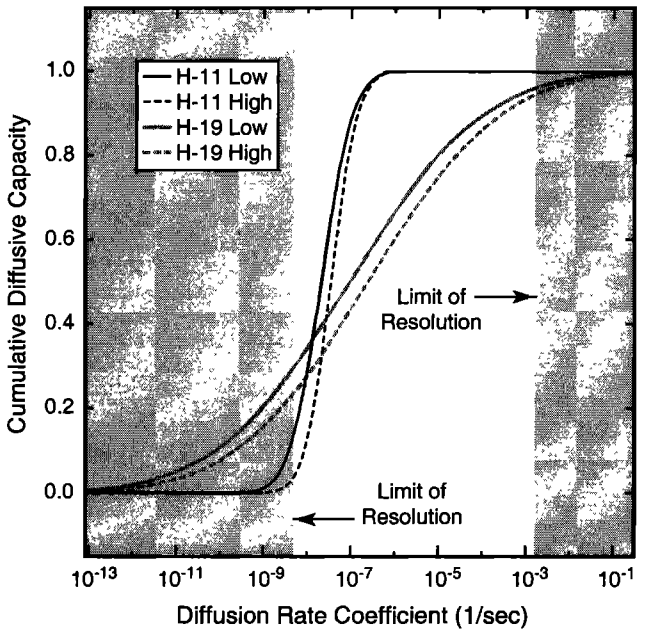

Figure 7. Cumulative distributions of diffusion rate coefficients as estimated from the four convergent-flow tracer tests. The open region shows the approximate limits of resolution for the multirate distributions.

magnitude decrease in time from the first observed data point and a 2-order-of-magnitude increase from the last observed data point in each tracer test will cover the range of diffusion rate coefficients that could possibly be observed during the test. This assumption is consistent with arguments based on Damkohler numbers (ratio of diffusive timescale to advective timescale) [e.g., *Bahr and Rubin*, 1987]. For example, in the H-19 high test the earliest observed data point is $3.9 \times 10^{+04}$ s. Dividing this time by 100 gives a conservative estimate of the fastest characteristic time for diffusion that could be observed in this test. The inverse of this estimate, 2.6×10^{-03} (1/s), gives the corresponding diffusion rate coefficient for this lower time limit. Diffusion rates faster than this limit can be considered instantaneous relative to the timescale of the tracer test. The diffusion rate coefficient corresponding to a characteristic time of diffusion that is 100 times longer than the time at which the last data point was observed in the H-19 high test is 4.0×10^{-09} (1/s). Diffusion rates slower than this limit could not be observed in the test, and the fraction of the diffusive capacity associated with these slower rates would appear as an infinite sink for solute over the timescale of the tracer tests.

These upper and lower limits on the resolution of the multirate distribution are calculated for each tracer test and compared to the estimated diffusion rate coefficient distributions in Figure 7. Although the upper and lower limits vary between tracer tests, the differences are slight, and thus only one upper and lower limit, applicable to all tests, are plotted on Figure 7. These limits are 1.5×10^{-03} and 5.0×10^{-09} (1/s) for the fastest and slowest diffusion rates, respectively. These limits are used to define three regimes of diffusion behavior: (1) rates faster than the upper limit of resolution corresponding to diffusive capacity that reaches equilibrium concentration with the advective porosity over the timescale of the test; (2) rates between the upper and lower limits of resolution corresponding to diffusive capacity that does not reach equilibrium with the advective porosity but has a nonzero concentration at the center of the diffusive porosity blocks; (3) rates below the lower limit of resolution where the diffusive capacity still acts as an infinite sink for solute. These three regimes can exist simultaneously in a multirate model but not in a single-rate model.

The portion of the lognormal distributions that can actually be resolved during the tests is determined by applying the time limits discussed above. At the H-11 hydropad, roughly 90–97% of the diffusion rate distribution lies within the time limits with just the slowest 3–10% of the rates lying below the lower limit of resolution. Inclusion of the majority of the distribution within the resolution limits results in relatively tight confidence intervals on the estimates of σ_d (Table 2). At the H-19 hydropad, approximately 70–75% of the distribution lies within the resolution limits (Figure 7). Consequently, at the H-19 hydropad ~20–25% of the estimated diffusion rates are so slow as to appear as infinite capacity for diffusion, and ~5% of the rates are fast enough to appear as instantaneous. The large confidence intervals about the estimates of σ_d, shown in Table 2 for H-19, are due to the proportion of the estimated diffusion rate coefficient distribution that lies outside the time limits. The distribution is effectively unestimable outside these limits and only has shape in those regions (Figure 7) because of the a priori assumption of a lognormal distribution.

A check on the consistency of the estimated, lognormal distributions of diffusion rate coefficients is to determine the estimated diffusion path length distribution. All variability in the diffusion rate coefficients is assigned to variations in diffusion path lengths by assuming a constant tortuosity and then comparing estimated diffusion path lengths to field observations of matrix blocks. For one-dimensional diffusion paths into the matrix the distance l from the fracture-matrix interface to the center of the matrix block (matrix block half length) can be calculated using the laboratory-derived values of D_{aq} and τ (Table 1) in equation (2b). The resulting distributions show that these tests were able to image, within the resolution limits, a range of half-block sizes from 2.3×10^{-04} to 0.13 m. These estimates of block size are consistent with the range of half-block sizes of $\sim 1 \times 10^{-04}$ to >0.30 m observed in core and observations made in the WIPP shafts [*Holt*, 1997, Plates 2–6 and 2–10]. These estimates are also consistent with the diffusion path length estimates of 2.6×10^{-04} to 0.19 m made with the SWIW data [*Haggerty et al.*, this issue].

The observed BTC data show similar peak concentrations for both pumping rates. This behavior is generally characteristic of a single-porosity aquifer, provided the difference in pumping rates is large enough to change the peak concentration significantly. Attempts at single-porosity matches to these CFTT results did not provide adequate fits to the observed data [*Kelley et al.*, 2000]. In a multirate system characterized by a lognormal distribution of diffusion coefficients, the change in peak height between different pumping rates decreases as σ_d increases. Using the parameters estimated at H-19 ($\sigma_d > 5.0$), numerical simulations show a constant peak height across pumping rates that change by up to 1 order of magnitude. Similar simulations using the parameters estimated at H-11 (σ_d near 1.0) show a change in peak concentration across the same range of pumping rates. We are currently evaluating different parametric and nonparametric, including bimodal, distributions of diffusion coefficients to understand better the similarity in peak concentrations across different pumping rates.

Table 3. Values of Parameters Estimated Using a Single-Rate Convergent Flow Model

Test	n	μ_d	σ_d	ϕ_a	α_L, m	ϕ_d	RMSE
H-11 low	107	−19.5	0.0	8.2×10^{-04}	2.4	0.16	0.18
H-19 low	67	−21.1	0.0	5.7×10^{-02}	2.4	0.094	0.16

3.4. Single-Rate, Double-Porosity Model

Previous to this work, only single-valued diffusion rates have been applied to the analysis of CFTTs in double-porosity media. To compare the results of the multirate model to the conventional, single-rate (double porosity) approach, single-rate model runs were completed using parameter estimation for the low pumping rate tracer test at each hydropad. This estimation procedure is the same as that used for the multirate model; however, σ_d is set to 0.0. In order to be consistent with the SWIW results the single-rate diffusion is modeled as diffusion into spheres [see *Haggerty et al.*, this issue]. In order to maintain consistency these single-rate runs were constrained to have the same total porosity ($\phi_a + \phi_d$) as derived from the multirate modeling. Results of the single-rate matches to the observed data are given in Table 3 and Figures 8 and 9. As measured by the RMSE, the multirate model provides a better fit to the data than does the single-rate model for both the H-11 and H-19 tests. The RMSE is approximately a factor of 2 lower for the multirate model of the H-11 data; however, the improvement in the fit to the data is only marginal for the H-19 test.

In general, the estimated single rate of mass transfer is smaller (larger negative number) than the mean of the multirate distribution for both of the CFTTs modeled. The estimated mass transfer rate using the conventional double-porosity model results in diffusive path lengths of 0.16 and 0.32 m at the H-11 and H-19 hydropads, respectively. Both of the diffusion rate coefficients estimated with the single-rate models fall below the lower-resolution limit calculated above. The values of the estimated diffusion rate coefficients (Table 3) calculated with a single-rate model are 3.4×10^{-09} and 6.9×10^{-10} (1/s) for the H-11 and H-19 tests, respectively. For the length of time that these tracer tests were run, these single diffusion rate coefficients will produce a model with infinite capacity behavior.

Conversely, the multirate model estimated relatively rapid to instantaneous rates for a fraction of the total porosity. In the H-11 multirate models none of the diffusive capacity reaches equilibrium with the advective porosity, and a small fraction of the diffusive porosity acts as an infinite sink for solute (Figure 7). The H-19 multirate results show that some fraction of the diffusive porosity achieves equilibrium with the concentration in the advective porosity (fraction above the upper limit of resolution in Figure 7). The majority of the diffusive porosity is between the limits of resolution, and some fraction of the diffusive porosity still acts as an infinite sink for solute (below the lower limit of resolution).

For the H-19 test the advective porosity estimated with a single-rate model is over an order of magnitude larger than that estimated with the multirate model (Table 3). This increase in the advective porosity for the H-19 single-rate results is interpreted as the assignment of the fraction of diffusive capacity that reaches equilibrium in the multirate model as advective porosity in the single-rate model. The upper limit of rate coefficient resolution shows that none of the diffusive capacity reaches equilibrium for the H-11 data. Therefore it is not necessary to increase the advective porosity estimate in order to match the H-11 data with a single-rate model. The consistency of these results with the limits of resolution shown in Figure 7 provides additional confidence in the choice of the multirate conceptual model.

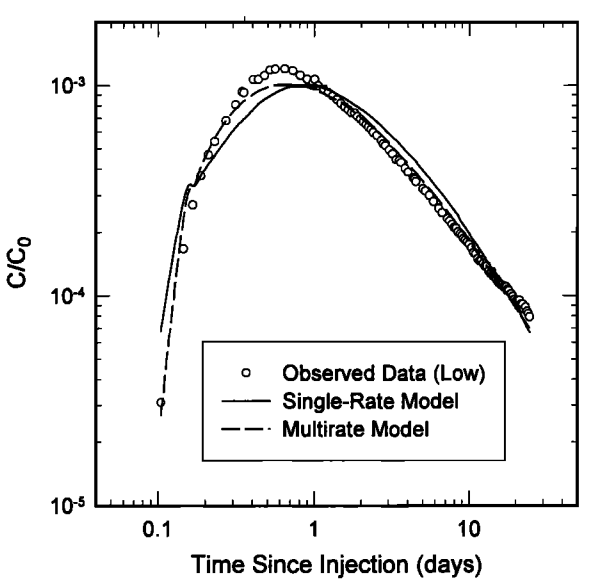

Figure 8. Single-rate model fit to the H-11 low data. The multirate model fit is shown for comparison.

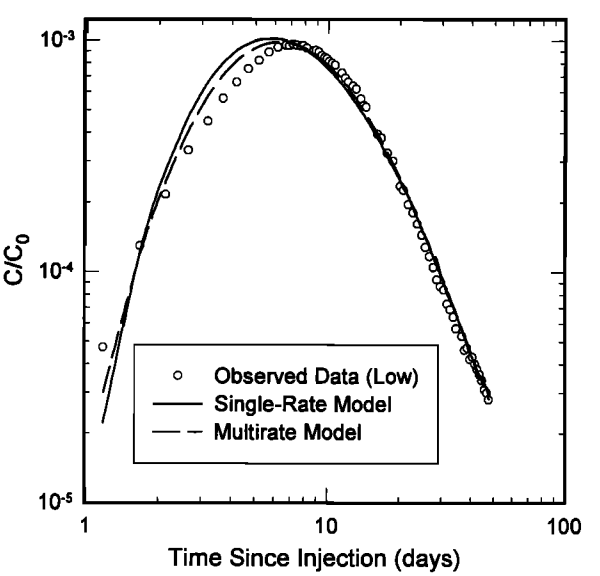

Figure 9. Single-rate model fit to the H-19 low data. The multirate model fit is shown for comparison.

4. Uniqueness and Testing of the Estimated Models

A test of the robustness or validity of the estimated multirate transport model is to use the transport parameters estimated at one pumping rate to model the observed BTC at the other pumping rate. If the conceptual model of a continuous distribution of diffusion rate coefficients holds, the change in pumping rate will shift the portion of the diffusion rate coefficient distribution that the test is able to see (that region between seemingly infinite block size and equilibrium behavior). However, if the single mass transfer rate model applies, there are no other rates to shift to with changing pumping. If this change is significant, then matching the BTC using transport parameters from tests at a different pumping rate will not be possible.

The observed data at the higher pumping rates are modeled using both the continuous distribution of diffusion rates estimated at the lower pumping rate and also using the single diffusion rate estimated at the lower pumping rate with a single-rate model. The results of these runs are shown with the observed data in Figures 10 and 11. The RMSE for the fits shown in Figure 10 (H-11 tracer test) are 0.26 and 0.30 for the single-rate and multirate models, respectively. The RMSE values for the models shown in Figure 11 (H-19 tracer test) are 0.33 and 0.24 for the single-rate and multirate models, respectively. In both cases the single-rate model estimated at the lower pumping rate is capable of matching the data observed at the higher pumping rate as well as the multirate model. Also, the fits to the H-19 data are better than the model fits to the H-11 data for both the single-rate and multirate models. If a larger difference in pumping rates had been used in the field test, it might have been possible to differentiate between the two models.

Another test of the model would be to use the transport parameters estimated on one BTC to estimate a BTC from another tracer with a significantly different aqueous diffusion coefficient. Iodide was chosen as an additional tracer for the H-19b7 tracer test because it has an aqueous diffusion coefficient that is approximately a factor of 2–3 larger than the benzoic acids and it has a low background concentration in the Culebra brines. The peaks of the iodide BTCs are lower than those of the benzoic acids for the H-19b7 tracer test [see *Meigs and Beauhem*, this issue]; however, the uncertainty in the iodide concentrations is much higher than those of the benzoic acids. This uncertainty led to extremely nonunique fits to the iodide data using the multirate and single-rate models. The results of these models are not presented here.

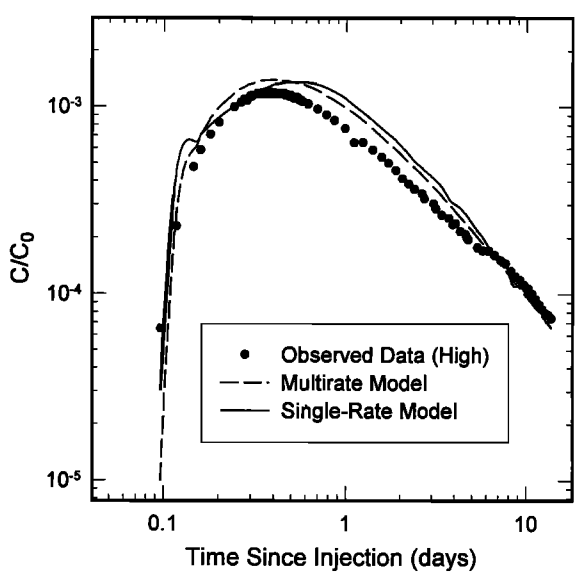

Figure 10. Model fits to the H-11 high tracer test data using both multirate and single-rate models estimated on the H-11 low tracer test data.

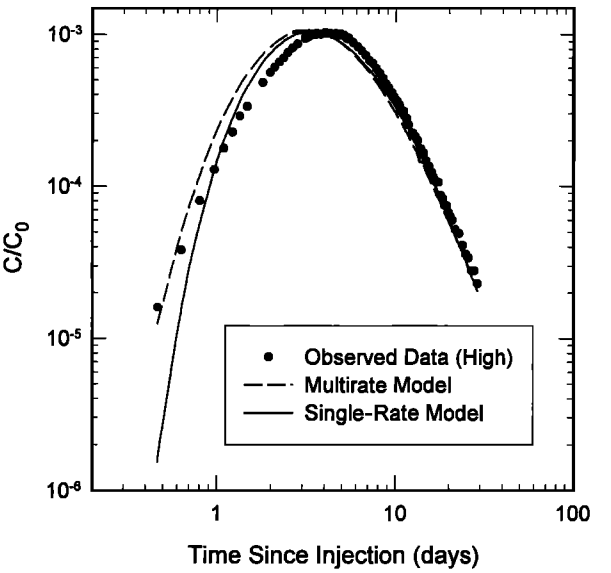

Figure 11. Model fits to the H-19 high tracer test data using both multirate and single-rate models estimated on the H-19 low tracer test data.

5. Comparison of SWIW and CFTT Results

Results of modeling the CFTTs are compared to those of the SWIW tests with the goal of understanding the differences in the estimated parameters in terms of the differences in the two tracer test designs. We do not expect that the results of the different tests will be identical because of the different test geometries and, to a large extent, nonoverlapping volumes of aquifer being tested. Additionally, the CFTTs are more sensitive to ϕ_a and α_L than are the SWIW tests. For example, the SWIW test is completely insensitive to the value of advective porosity [*Haggerty et al.*, this issue, see Table 3], but ϕ_a is estimated with relatively tight confidence intervals by models of the CFTTs (Table 2). The similarities of the diffusion rate coefficient distributions estimated at the same hydropad, but with different pumping rates, and the differences in the estimated distributions between hydropads as seen in the SWIW tests are also seen in the distributions estimated with the CFTT results. In both the SWIW and CFTT results the diffusion rate coefficient distribution has a lower mean and smaller deviation when estimated with the H-11 data compared to the estimates made with the H-19 data.

Comparison of Table 2 of *Haggerty et al.* [this issue] with Table 2 in this paper shows that the estimates of μ_d from the SWIW tests and the CFTTs are similar at H-11 and quite different at H-19. At H-19 the estimates of the mean diffusion rate coefficient by the SWIW model are approximately 2 orders of magnitude higher than those estimated by the CFTT model. One explanation for the large differences between the

SWIW and CFTTs at H-19 is the time available for diffusion. The normalized sensitivities (see Figure 4) indicate that for times beyond the peak concentration the main process affecting the BTC is diffusion back out of the diffusive porosity into the advective porosity. The elapsed time from beginning of tracer collection to peak concentration in the BTC is used as a representative time for diffusion into the diffusive porosity to occur. At H-11 this representative time is approximately 75,000 s for the SWIW test and is roughly 45,000 s for the CFTT. However, at H-19 this representative time for diffusion is almost an order of magnitude longer in the CFTT (3.5×10^5 to 6.0×10^5 s) than in the SWIW tests (approximately 75,000 s). These similar times for diffusive mass transfer at H-11 across both tests result in models that predict similar values for μ_d (see Table 2). The longer time for diffusion in the H-19 CFTT relative to the SWIW tests allows the tracer to sample slower diffusion rates, and these slower rates significantly decrease the estimated mean of the diffusion rate coefficient distribution relative to the SWIW test.

6. Mass Transfer Processes at Larger Scales

The final goal of determining mass transfer rates within the Culebra dolomite, and many aquifers examined by tracer testing, is use of the estimated parameters in a solute transport model for predictions of transport processes at larger spatial and temporal scales. These calculations may be performed on spatial scales of kilometers and temporal scales of hundreds to thousands of years. This raises the question of the effect a multirate mass transfer process might have on the shape of a solute plume at various distances downgradient of the solute source relative to that predicted by a conventional single-rate double-porosity model. Specifically, does the solute reach an equilibrium concentration throughout the entire diffusive capacity or only some fraction of this capacity?

At larger time and length scales, two differences between the single-rate and multirate models estimated in this work must be considered: (1) Single-rate models may indicate a larger advective porosity than do the multirate models. (2) Slow rates in the tail of the multirate diffusion coefficient distribution may cause at least a fraction of the diffusive porosity to remain in disequilibrium with the advective porosity solute concentration even at very large times. The first difference in conceptual models is not significant at long timescales as the solute concentration in the advective porosity comes to equilibrium within a large portion of the diffusive capacity relatively quickly. The significance of the slow rates in the tail of the distribution is analyzed by using the estimated distributions of diffusion rate coefficients and the resolution limits and calculating similar resolution limits on the diffusion rate coefficients for the timescales associated with the transport distances of 300 and 3000 m. These distances represent one tenth the expected flow path length and the expected flow path length to the WIPP compliance boundary, respectively.

A specific discharge of 1×10^{-10} m/s (see range of values given by *LaVenue et al.* [1990]) is used to determine the advective travel times. This specific discharge results in advective velocities of approximately 2.7×10^{-08} to 1.6×10^{-07} m/s using the advective porosity estimates in Table 2. Taking an average velocity of 9.35×10^{-08} m/s, the times necessary for the groundwater to travel 300 and 3000 m are $3.2 \times 10^{+09}$ and $3.2 \times 10^{+10}$ s, respectively. The diffusion rate coefficient corresponding to the inverse of these 300 and 3000 m advective travel times, 3.1×10^{-10} and 3.1×10^{-11} (1/s), respectively, are below the lower limit of rate coefficients that could be resolved from the tracer tests.

In order to better understand the effects of multirate transport at larger scales the fractions of the diffusive capacity distributions estimated with the H-11 and H-19 low tracer tests that will have come to equilibrium and that will still appear as infinite sinks after exposure times of $3.2 \times 10^{+09}$ and $3.2 \times 10^{+10}$ s, respectively, are determined. In a solute release scenario the volume of rock very close to the solute source will experience these exposure times. This determination is done by calculating the plus and minus 2-orders-of-magnitude bounds on the advective travel times for the 300 and 3000 m travel distances. These calculations produce upper and lower bounds on the diffusion rate coefficients of 3×10^{-08} and 3×10^{-12} (1/s) for the $3.2 \times 10^{+09}$ s exposure time and 3×10^{-09} and 3×10^{-13} (1/s) for the $3.2 \times 10^{+10}$ s exposure time. The fraction of the distribution above the upper bound is considered to be diffusive porosity that has reached equilibrium with the concentration in the advective porosity after this amount of exposure time. The fraction of the diffusive porosity below the lower bound is still acting as an infinite sink for solute at these timescales.

For the rate coefficient distributions estimated with the H-11 data, after $3.2 \times 10^{+09}$ s, approximately 60% of the diffusive porosity will have reached an equilibrium concentration with the concentration in the advective porosity. None of this diffusive porosity will still be acting as an infinite sink for solute. After $3.2 \times 10^{+10}$ s, approximately 98% of the diffusive porosity will have reached equilibrium with the advective porosity concentration. For the broader diffusion rate coefficient distribution estimated with the H-19 data, approximately 65% of the diffusive porosity at the solute source will have reached equilibrium after $3.2 \times 10^{+09}$ s and approximately 3% of the diffusive porosity will still act as an infinite sink for solute. After $3.2 \times 10^{+10}$ s, roughly 80% of the diffusive porosity at the source location will have reached equilibrium, and only 1% will still behave as an infinite sink.

This simple exercise affords three important insights into multirate solute transport at larger scales. First, these results point out an inherent difficulty in deriving transport parameter information that is useful for predictions at large temporal and spatial scales from tracer tests conducted at much shorter scales. One solution may be to supplement information derived from relatively short-scale tracer tests with geologic mapping, along the larger-scale transport pathway, of the spatial occurrence and proportion of different porosity types and matrix block sizes corresponding to different diffusion rate coefficients. Second, under a multirate conceptual model it may not be correct to assume that the entire diffusive (matrix) porosity has come to equilibrium with the solute concentration in the advective porosity at larger timescales. The fraction of the diffusive porosity associated with the slowest rates may still be acting as a sink of infinite capacity for solute even at very long times. Finally, it is not possible to accurately model transport in the Culebra, based on the H-19 tracer test results, with a single-porosity conceptualization. The single-porosity model, exhibiting complete equilibrium with the matrix, may be a nonconservative (i.e., low) estimate of the cumulative release of solute across a regulatory boundary.

7. Effects of Heterogeneity

Heterogeneity is not included in the application of this semi-analytical transport model to the CFTT results; however, heterogeneity must be addressed in any discussion of transport in the Culebra. In a convergent flow system, such as those used in the CFTTs modeled here, numerical studies [*McKenna*, 2000] indicate that the effect of heterogeneity alone on producing the tailing observed in the breakthrough curves is minimal. The main effect of heterogeneity in these tracer tests is to focus transport into preferential flow paths. This focusing could limit the applicability of the conceptual model used here that allows for simultaneous access of solute to the entire multirate distribution. Under significant focusing of flow, only those diffusion rates adjacent to the flow path will affect transport results. The effects of a spatially distributed diffusion rate coefficient distribution are beyond the scope of this study

Focused flow was suggested as a mechanism for the results observed in the SWIW tests at H-11 [*Haggerty et al.*, this issue]. The CFTT results provide additional evidence of focused flow at the H-11 hydropad relative to the H-19 hydropad. For the H-11 and H-19 low pumping rate tests the pumping rates are very similar (Table 1). Even with a significantly longer distance between the injection and pumping wells (Table 1) and similar estimates of advective porosity (Table 2), the time to peak arrival at the H-11 hydropad is an order of magnitude shorter than the peak arrival time of the H-19 results (Figures 2 and 3). This result is further evidence of preferential flow at H-11 relative to H-19. The main result of this preferential flow is a narrower distribution of diffusion rate coefficients estimated at H-11 relative to H-19 (Figure 7). Similar results were observed in the SWIW tests [*Haggerty et al.*, this issue]

Under ambient flow conditions at larger scales, focusing of flow will be less prevalent than in the CFTTs, and the solute will experience a wider distribution of diffusion rate coefficients. At the small scale the heterogeneous distribution of transmissivity and the ambient flow field may create localized zones of matrix porosity acting as advective porosity. This effect will further blur the distinction between diffusive and advective porosity and may contribute to advective mass transfer into the matrix porosity.

8. Conclusions

The multirate diffusion model developed previously [*Haggerty and Gorelick*, 1995] is extended to the case of a convergent flow system with an injection at some distance from the pumping well. This model has been applied to a portion of the results from the H-11 and H-19 tracer tests conducted in the Culebra dolomite at the WIPP site. Parameters estimated from modeling the observed data suggest that the diffusion behavior is different from one hydropad to the other. At H-11 the confidence intervals on the estimated σ_d values are relatively tight, while the confidence intervals on σ_d at H-19 are quite large and indicate that σ_d is unestimable at H-19. For the pathway evaluated at the H-11 hydropad, the estimated values of α_L are greater than 15% of the length of the transport pathway, while for the pathway evaluated at the H-19 hydropad these values are less than 10% of the pathway length. The confidence intervals on ϕ_a are narrow at both hydropads.

Results of this work indicate that evidence of multirate diffusion is best determined by the SWIW tracer test. In a SWIW test the effects of flow field heterogeneity are mitigated, and the signature of multirate diffusion is easily detectable. In the case of the CFTT both a single-rate and multirate model are capable of describing the observed data. The added effects of flow field heterogeneity creating preferential flow paths and correlation of the mean diffusion rate with the advective porosity in the CFTT make the interpretation of the diffusion process more ambiguous. However, the CFTT is capable of providing information on the position (mean) and shape of the multirate distribution that is consistent with the SWIW test across both hydropads.

Parameters derived with data from a SWIW test are not necessarily transferable to a CFTT. The fast end of the diffusion rate distribution is better estimated with a SWIW test because of the insensitivity of that test to advective porosity. For a CFTT it can be difficult to differentiate the effects of very fast diffusion rates from advective porosity. At H-19 the insensitivity of the SWIW test to advective porosity made it impossible to simulate the test data with a single-rate model. The H-19 CFTT can be simulated with a single-rate model by using an increased advective porosity to account for the diffusive porosity that reaches equilibrium during the test. For the H-11 CFTT results none of the capacity reaches equilibrium during the test, and the single-rate models produce an advective porosity estimate similar to that of the multirate model.

At larger transport scales the width of the estimated multirate diffusion coefficient distribution will dictate whether or not a single-porosity model can accurately model the transport behavior for a given transport distance. On the basis of the parameters estimated in this work, a single-rate conceptualization may predict a smaller cumulative release across a regulatory boundary, relative to a multirate model, because of the entire matrix capacity reaching equilibrium with the fracture concentration. If very slow diffusion rates are present in the multirate model, a fraction of the matrix may not reach an equilibrium concentration, and the predicted cumulative releases across the regulatory boundary will be larger. A matrix that has not reached the equilibrium concentration can also be maintained at larger scales with a single-rate model if a slower diffusion rate is chosen. At large transport scales the fraction of the diffusive porosity associated with fast diffusion rates will have reached equilibrium. Whether this fraction of the total capacity is accounted for explicitly in the transport model or just assigned as advective porosity does not make a difference for the cases examined here. Heterogeneity can focus flow in CFTTs as evidenced in the H-11 results. This focused flow may cause underestimation of true value of σ_d.

Notation

b aquifer thickness $[L]$.

$b(\alpha_d)$ probability density function of diffusion rate coefficients [dimensionless].

c_a solute concentration in the advective porosity $[M/L^3]$.

$\hat{C}_d(\alpha_d)$ average solute concentration in the portion of the diffusive porosity $[M/L^3]$.

c_d concentration at a point within a portion of the diffusive porosity $[M/L^3]$.

D_{aq} aqueous (free water) diffusion coefficient $[L^2/T]$.

D_a apparent matrix diffusion coefficient $(D_{\text{aq}}\,\tau)$ $[L^2/T]$.

l length of the diffusion pathway within the matrix $[L]$.

Q_{inj} rate of injection for the tracer or chaser $[L^3/T]$.

Q_{out} discharge rate of the pumping well $[L^3/T]$.
R_a retardation factor within the advective porosity [dimensionless].
R_d retardation factor within the diffusive porosity [dimensionless].
r radial coordinate (positive away from well) $[L]$.
R_0 distance between the injection and pumping wells $[L]$.
r_w well radius (injection or pumping $[L]$.
T elapsed time since the beginning of tracer injection $[T]$.
t time $[T]$.
z coordinate along the one-dimensional diffusion pathway $[L]$.
α_d continuously distributed diffusion rate coefficient $[1/T]$.
α_L longitudinal dispersivity along flow path $[L]$.
β_{tot} total capacity coefficient of the formation [dimensionless].
ϕ_a advective porosity of the formation [dimensionless].
ϕ_d diffusive porosity of the formation [dimensionless].
μ_d mean of the log-transformed diffusion rate coefficients $[1/T]$.
σ_d standard deviation of the log-transformed diffusion rate $[1/T]$.
τ diffusive tortuosity [dimensionless].
v instantaneous pore water velocity at a distance r along a flow path $[L/T]$.

Acknowledgments. Sandia is a multiprogram laboratory operated by Sandia Corporation, a Lockheed Martin Company, for the United States Department of Energy under contract DE-AC04-94AL85000. This paper was improved through the reviews of V. Tidwell, T. Corbet, P. Davies, R. Beauheim, G. de Marsily, L. Konikow, P. Maloszewski, A. Zuber, and an anonymous reviewer and discussions with S. Altman, S. Fleming, and R. Holt. Some of the calculations herein were done by M. Kelley, T. Jones, and J. Ogintz.

References

Altman, S. J., T. L. Jones, and L. C. Meigs, Controls on mass recovery for single-well injection-withdrawal tracer, in *Interpretations of Tracer Tests Performed in the Culebra Dolomite at the Waste Isolation Pilot Plant Site*, edited by L. C. Meigs, R. L. Beauheim, and T. L. Jones, chap. 4, pp. 37–68, *Rep. SAND97-3109*, Sandia Natl. Lab., Albuquerque, N. M., 2000.

Bahr, J. M., and J. Rubin, Direct comparison of kinetic and local equilibrium formulations for solute transport affected by surface reactions, *Water Resour. Res.*, *23*(3), 438–452, 1987.

Cunningham, J. A., C. J. Werth, M. Reinhard, and P. V. Roberts, Effects of grain-scale mass transfer on the transport of volatile organics through sediments, 1, Model development, *Water Resour. Res.*, *33*(12), 2713–2726, 1997.

D'Alessandro, D., F. Mousty, G. Bidoglio, J. Guimerà, I. Benet, X. Sánchez-Vila, M. García Gutiérrez, and A. Yllera De Llano, Field tracer experiment in a low permeability fractured medium: Results from El Berrocal site, *J. Contam. Hydrol.*, *26*, 189–201, 1997.

García Gutiérrez, M. G., J. Guimerà, A. Yllera De Llano, A. Hernàndez Benitez, J. Humm, and M. Saltink, Tracer test at El Berrocal site, *J. Contam. Hydrol.*, *26*, 179–188, 1997.

Guvanasen, V., and V. M. Guvanasen, An approximate semianalytical solution for tracer injection tests in a confined aquifer with a radially converging flow field and finite volume of tracer and chase fluid, *Water Resour. Res.*, *23*(8), 1607–1619, 1987.

Hadermann, J., and W. Heer, The Grimsel (Switzerland) migration experiment: Integrating field experiments, laboratory investigations and modeling, *J. Contam. Hydrol.*, *21*, 87–100, 1996.

Haggerty, R., Laplace-domain solution for multirate model, in *Interpretations of Tracer Tests Performed in the Culebra Dolomite at the Waste Isolation Pilot Plant Site*, edited by L. C. Meigs, R. L. Beauheim, and T. L. Jones, Append. Q, *Rep. SAND97-3109*, Sandia Natl. Lab., pp. 351–353, Albuquerque, N. M., 2000.

Haggerty, R., and S. M. Gorelick, Multiple rate mass transfer for modeling diffusion and surface reactions in media with pore-scale heterogeneity, *Water Resour. Res.*, *31*(10), 2383–2400, 1995.

Haggerty R., and S. M. Gorelick, Modeling mass transfer processes in soil columns with pore-scale heterogeneity, *Soil Sci. Soc. Am. J.*, *62*(1), 62–74, 1998.

Haggerty, R., S. W. Fleming, L. C. Meigs, and S. A. McKenna, Tracer tests in a fractured dolomite, 2, Analysis of mass transfer in single-well injection-withdrawal tests, *Water Resour. Res.*, this issue.

Harvey, J. W., B. J. Wagner, and K. E. Bencala, Evaluating the reliability of the stream tracer approach to characterize stream-subsurface water exchange, *Water Resour. Res.*, *32*(8), 2441–2451, 1996.

Hollenbeck, K. J., C. F. Harvey, R. Haggerty, and C. J. Werth, Estimation of continuous mass-transfer rate distributions, *J. Contam. Hydrol.*, *37*, 367–388, 1999.

Holt, R. M., Conceptual model for transport processes in the Culebra Dolomite Member, Rustler Formation, *Rep. SAND97-0194*, Sandia Natl. Lab., Albuquerque, N. M., 1997.

Kelley, M. J., L. C. Meigs, R. L. Beauheim, S. A. McKenna, and R. Haggerty, Double-porosity single-rate and multirate interpretations of multiwell convergent-flow tracer-test data, in *Interpretations of Tracer Tests Performed in the Culebra Dolomite at the Waste Isolation Pilot Plant Site*, edited by L. C. Meigs, R. L. Beauheim, and T. L. Jones, Append. S, pp. 363–407, *Rep. SAND97-3109*, Sandia Natl. Lab., Albuquerque, N. M., 2000.

LaVenue, A. M., T. L. Cauffman, and J. F. Pickens, Ground-water flow modeling of the Culebra dolomite, in *Model Calibration*, vol. I, *Rep. SAND89-7068/1*, Sandia Natl. Lab., Albuquerque, N. M., 1990.

Maloszewski, P., and A. Zuber, Tracer experiments in fractured rocks: Matrix diffusion and the validity of models, *Water Resour. Res.*, *29*(8), 2723–2735, 1993.

McKenna, S. A., Controls on multiwell convergent-flow tracer-breakthrough-curve tailing for a single-porosity, heterogeneous conceptualization, in *Interpretations of Tracer Tests Performed in the Culebra Dolomite at the Waste Isolation Pilot Plant Site*, edited by L. C. Meigs, R. L. Beauheim, and T. L. Jones, *Rep. SAND97-3109*, chap. 5, pp. 69–83, Sandia Natl. Lab., Albuquerque, N. M., 2000.

Meigs, L. C., and R. L. Beauheim, Tracer tests in a fractured dolomite, 1, Experimental design and observed tracer recoveries, *Water Resour. Res.*, this issue.

Moench, A. F., Convergent radial dispersion: A Laplace transform solution for aquifer tracer testing, *Water Resour. Res.*, *25*(3), 439–447, 1989.

Moench, A. F., Convergent radial dispersion in a double-porosity aquifer with fracture skin: Analytical solution and application to a field experiment in fractured chalk, *Water Resour. Res.*, *31*(8), 1823–1835, 1995.

Neretnieks, I., and A. Rasmuson, An approach to modeling radionuclide migration in a medium with strongly varying velocity and block sizes along the flow path, *Water Resour. Res.*, *20*(12), 1823–1836, 1984.

Novakowski, K. S., G. V. Evans, D. A. Lever, and K. G. Raven, A field example of measuring hydrodynamic dispersion in a single fracture, *Water Resour. Res.*, *21*(8), 1165–1174, 1985.

Sánchez-Vila, X., and J. Carrera, Directional effects on convergent flow tracer tests, *Math. Geol.*, *29*(4), 551–569, 1997.

Wagner, B. J., and J. W. Harvey, Experimental design for estimating parameters of rate-limited mass transfer: Analysis of stream tracer studies, *Water Resour. Res.*, *33*(7), 1731–1741, 1997.

Welty, C., and L. W. Gelhar, Evaluation of longitudinal dispersivity from nonuniform flow tracer tests, *J. Hydrol.*, *153*, 71–102, 1994.

Zlotnik, V. A., and J. D. Logan, Boundary conditions for convergent radial tracer tests and effect of well bore mixing volume, *Water Resour. Res.*, *32*(7), 2323–2328, 1996.

R. Haggerty, Department of Geosciences, Oregon State University, 104 Wilkinson Hall, Corvallis, OR 97331-5506. (haggertr@ucs.orst.edu)

S. A. McKenna and L. C. Meigs, Geohydrology Department, Sandia National Laboratories, P.O. Box 5800, MS 0735, Albuquerque, NM 87185-0735. (samcken@sandia.gov; lcmeigs@sandia.gov)

(Received March 17, 2000; revised October 13, 2000; accepted October 16, 2000.)